538163

Resolving the Structure of Ionized Helium in the Intergalactic Medium with the Far Ultraviolet Spectroscopic Explorer

G.A. Kriss[1,2,*], J.M. Shull[3], W. Oegerle[4], W. Zheng[2], A.F. Davidsen[2], A. Songaila[5], J. Tumlinson[3], L.L. Cowie[5], J.-M. Deharveng[6], S.D. Friedman[2], M.L. Giroux[3], R.F. Green[7], J. Hutchings[8], E.B. Jenkins[9], J.W. Kruk[2], H.W. Moos[2], D.C. Morton[8], K.R. Sembach[2], T.M. Tripp[9],

Received _____; accepted _____

Version 2.3, May 18, 2001.

---

[1]Space Telescope Science Institute, 3700 San Martin Drive, Baltimore, MD 21218

[2]Center for Astrophysical Sciences, Department of Physics and Astronomy, The Johns Hopkins University, Baltimore, MD 21218–2686

[3]CASA and JILA, Department of Astrophysical and Planetary Sciences, University of Colorado, Campus Box 389, Boulder, CO 80309

[4]Laboratory for Astronomy and Solar Physics, Code 681, NASA/Goddard Space Flight Center, Greenbelt, MD 20771

[5]University of Hawaii, Institute for Astronomy, 2680 Woodlawn Road, Honolulu, HI 96822

[6]Laboratorie d'Astronomie Spatiale, BP 8, 13376 Marseille Cedex 12, France

[7]Kitt Peak National Observatory, National Optical Astronomy Observatories, P.O. Box 26732, 950 North Cherry Ave., Tucson, AZ, 85726-6732

[8]Dominion Astrophysical Observatory, National Research Council of Canada, Victoria, BC, V8X 4M6, Canada

[9]Princeton University Observatory Princeton, NJ 08544

* To whom correspondence should be addressed. E-mail: gak@stsci.edu

ABSTRACT

The neutral hydrogen and the ionized helium absorption in the spectra of high-redshift QSOs are unique probes of structure in the universe at epochs intermediate between the earliest density fluctuations seen in the cosmic background radiation and the distribution of galaxies visible today. We present *Far-Ultraviolet Spectroscopic Explorer (FUSE)* observations of the line of sight to the QSO HE2347–4342 in the 1000–1187 Å band at a resolving power of 15,000. Above redshift $z = 2.7$, the IGM is largely opaque in He II Lyα (304 Å). At lower redshifts, the optical depth gradually decreases to a mean value $\tau \sim 1$ at $z = 2.4$. We resolve the He II Lyα absorption as a discrete forest of absorption lines in the $z = 2.3 - 2.7$ redshift range. Approximately 50% of these spectral features have H I counterparts with column densities $N_{HI} > 10^{12.3}$ cm^{-2} visible in a Keck spectrum. These account for most of the observed opacity in He II Lyα. The remainder have $N_{HI} < 10^{12.3}$ cm^{-2}, below the threshold for current observations. A short extrapolation of the power-law distribution of H I column densities to lower values can account for these new absorbers. The He II to H I column density ratio η averages $\sim$80, consistent with photoionization of the IGM by a hard ionizing spectrum resulting from the integrated light of quasars at high redshift, but there is considerable scatter. Values of $\eta > 100$ in many locations indicate that there may be localized contributions from starbursts or heavily filtered QSO radiation.

Subject headings: Cosmology: Diffuse Radiation — Cosmology: Observations — Galaxies: Intergalactic Medium — Galaxies: Quasars: Individual (HE2347-4342) — Ultraviolet: General

The intergalactic medium (IGM) is the gaseous reservoir that provides the raw material for the galaxies that dominate our view of the visible universe. By observing distant bright objects such as quasars, we can explore the IGM by examining the absorption features it imprints on the light it transmits. The distribution of absorption features with redshift and the column density of material in different ions reveal the structure of the IGM and its density and ionization state. From the ionization state, we can also infer the processes responsible for ionizing the gas, e.g., radiation from quasars in the early universe, or from early bursts of star formation.

Searches for Lyα absorption by neutral hydrogen (Gunn & Peterson 1965) quickly led to the conclusion that any diffusely distributed gas must be too highly ionized to be visible. Discrete absorption features were common, however, and so plentiful that they were dubbed the "Lyman α forest" (Lynds 1971). Since ionized helium (He^+) requires more energy to ionize (54.4 eV) than hydrogen (13.6 eV) and recombines faster, its abundance in the IGM is expected to be higher. Searches for a diffuse component of the IGM therefore concentrated on the expected absorption from He II Lyα λ304 (Jakobsen et al. 1993). This absorption was first observed using the *Hubble Space Telescope (HST)* (Jakobsen et al. 1994) along the line of sight to the quasar Q0302-003 ($z = 3.29$). It showed the IGM to be essentially opaque at redshifts of $z \sim 3$, and it seemed possible that the material in the H I Lyα forest was sufficient to account for the He II opacity (Songaila et al. 1995; Heap et al. 2000). However, since no discrete He II features could be observed, this required several assumptions. The first measurement (rather than an upper limit) of the He^+ opacity, using the *Hopkins Ultraviolet Telescope (HUT)*, showed a translucent medium with He II optical depth $\tau \sim 1$ at $z \sim 2.4$ (Davidsen et al. 1996). The *HUT* observations were of insufficient spectral resolution to detect discrete He II absorption features. However, models of the

sightline towards HS1700+64 ($z = 2.72$) required a substantial contribution to the He II opacity from He^+ that was more smoothly distributed than the known H I Lyα absorbers (Davidsen et al. 1996; Zheng et al. 1998). Resolution of these inconsistencies requires observations at higher spectral resolution.

Recent theoretical studies have led to a compelling physical picture of the high-redshift IGM as a tracer of cosmic structure formation via gravitational instability. Diffusely distributed baryonic material (the protons and neutrons that constitute ordinary matter) responds to the gravitational influence of the underlying dark matter. The most overdense regions collapse first to form the earliest galaxies, but the moderately overdense and the underdense regions (the IGM) that fill 80% of the volume of the universe should contain ~50% of the baryons. Rather than being a uniform medium filling the space between galaxies, the IGM itself should be structured on large (compared to galactic) scales. Both numerical calculations (Cen et al. 1994; Zhang et al. 1995; Zhang et al. 1997; Hernquist et al. 1996; Miralda-Escudé et al. 1996; Croft et al. 1997; Cen & Ostriker 1999; Davé et al. 1999) and analytic theory (Bi 1993; Bi et al. 1995; Bi & Davidsen 1997; Hui et al. 1997) link the evolving structure of the IGM to the H I and He II absorption visible in the spectra of high redshift quasars.

Given the unsettled observational issues and the need to test the theoretical expectations, we planned high spectral resolution observations of the He II absorption toward the bright (V = 16.1) $z = 2.885$ quasar HE2347–4342 using the *Far Ultraviolet Spectroscopic Explorer (FUSE)*. Previous observations of HE2347–4342 showed it to be one of the brightest candidates for such observations (Reimers et al. 1997; Smette et al. 2001). As with the other quasars observed with *HST*, the He II absorption in this object is largely opaque, but there are wavelength intervals of high transmission that suggest we can see the beginnings of the He^+ re-ionization in the IGM in the redshift range visible toward this

quasar (Reimers et al. 1997). Since He II Lyα at $z = 2.885$ is redshifted to 1181 Å and *HST*/STIS is only sensitive down to 1150 Å, which corresponds to $z = 2.8$, the *HST* data do not cover a large range in redshift. We therefore hoped to trace this re-ionization process over a greater range with *FUSE* since its short-wavelength sensitivity would let us probe the IGM to much lower redshifts, down to $z \sim 2.1$ in principle.

FUSE covers the 912–1187 Å wavelength range at a resolving power of ~15,000 with four separate optical channels (Moos et al. 2000; Sahnow et al. 2000). Each channel consists of an off-axis paraboloidal mirror feeding a prime-focus Rowland circle spectrograph. The dispersed light is focused on two, two-dimensional photon-counting microchannel-plate detectors with KBr photocathodes that record the time, position, and pulse height of each photon event. Each detector is split into two segments (named A and B) with a small gap between them. Two channels (LiF1 and LiF2) use LiF-coated optics to cover the 1000–1187 Å band; the other two channels (SiC1 and SiC2) use SiC coatings to provide shorter-wavelength coverage down to 912 Å.

We observed HE2347–4342 with *FUSE* in two separate intensive campaigns. Since the count rate in a short observation in 2000 June was lower than the typical background rate, we chose the dates of these intensive observations to maximize the exposure time during orbital night when the background contribution due to scattered geocoronal Lyα is minimized. The first observation, from 2000 August 17 to 27, comprised 351,672 s of on-target time, of which 192,610 s was during orbital night. The second, running from 2000 October 11 to 21, accumulated 249,717 s on target, with 183,630 s at night. For each observing campaign, HE2347–4342 was centered in the $30'' \times 30''$ apertures. To maintain the optical alignment of the four channels during these campaigns, we periodically offset *FUSE* to the nearby UV-bright star WD2331–475 and performed routine adjustments to the mirror positions.

At the faint flux levels presented by HE2347–4342 ($F_\lambda \sim 3 \times 10^{-15}$ erg cm^{-2} s^{-1} Å^{-1} at 1200 Å, and fainter at wavelengths shortward of redshifted He II Lyα at $z = 2.89$), an accurate extraction of a background-subtracted, calibrated source spectrum from the two-dimensional recorded data required customized processing. Since the LiF channels have a throughput that is ~3 times higher than the SiC channels, we will only discuss the LiF portions of the spectrum in the remainder of this paper. Our discussion here is brief, and full details will be presented in a following paper (Shull et al. 2001). We first filtered high background "bursts" (Sahnow et al. 2000) from the data and eliminated all observation times outside orbital night. To reduce the background further, we used only events with pulse heights in the range 4–16. This reduces noise due to the low pulse-height events that arise from internal detector background rather than real photons. The standard *FUSE* data-processing pipeline subtracts a uniform background from each detector image before performing geometric rectification and extracting the source spectrum. The two-dimensional character of the *FUSE* detectors, however, makes it possible to subtract the background more accurately. Since there are spatial variations in the background that are significant in a source as faint as HE2347–4342, we turned off the standard background subtraction in the pipeline and extracted a "source + background" spectrum. We then manually extracted background spectra from the geometrically rectified detector images using regions lying adjacent to the source spectrum. Dead spots and airglow lines from other *FUSE* apertures were masked out of these background spectra. We computed a linear slope joining the two background regions, and scaled the final result for each of the four detector segments to match the level at the location of the extracted source+background spectrum. We subtracted these background spectra from the pipeline-extracted source+background spectra, and then used the rest of the normal pipeline processes to perform the standard wavelength and flux calibrations. At all steps in this process we propagated a 1-σ error array along with the data.

The multiplicity of detectors in *FUSE* and our two separate observations permit us to make a number of checks on our reduction process. At each wavelength we have two separate extracted spectra from each observation for a total of four independent spectra. All spectral features noted in our combined spectrum are visible in each independent spectrum. As a check on our flux levels, we compute the scatter among the fluxes from the 1000–1080 Å spectra (LiF1A and LiF2B) and the 1100–1187 Å spectra (LiF1B and LiF2A). For the former, it is 2.7×10^{-16} erg cm^{-2} s^{-1} Å^{-1}, and for the latter it is 2.1×10^{-16} erg cm^{-2} s^{-1} Å^{-1}. For both, it is higher than our 1-σ errors, indicating some residual systematic errors in our data reduction process. These errors are ~5–10% of the extrapolated continuum flux for HE2347–4342, and we take them as an indication of our overall uncertainty. As a check on our zero levels, we note that the interstellar absorption line of C II λ1036 is saturated in all *FUSE* extragalactic spectra. All four extracted spectra containing this line (LiF1A and LiF2B in each of the two separate observations) have zero flux at line center to within the 1-σ error bars. At wavelengths >1150 Å, prior GHRS and STIS observations of HE2347–4342 show several regions where there is little or no flux. Again, our extracted spectra also show no net flux in these regions to within our 1-σ errors.

Given the consistency among these separate observations, to maximize the signal-to-noise for further analysis, we combined the separate spectra into a single spectrum with a uniform wavelength scale and 0.05 Å bins. This combined spectrum is illustrated in Figure 1. Bins of 0.05 Å at the peak positive fluxes visible in Figure 1 have a signal-to-noise ratio of ~7.

Since the *FUSE* bandpass stops short of wavelengths where the unobscured continuum of HE2347–4342 is visible ($\lambda > 1190$ Å), we obtained low-resolution *HST*/STIS spectra contemporaneously with the *FUSE* observations to establish the continuum level. On 2000 August 21 and 2000 October 16, we obtained spectra covering 1150–3200 Å. These

observations each consisted of a 1060 s exposure using G140L and the FUV-MAMA and a 600 s exposure using G230L and the NUV-MAMA. HE2347-4342 was slightly but significantly fainter (by 7%) in the October observation, but otherwise the spectra were identical. We scaled the October observation up to the August flux levels, and fitted a simple power law with an extinction correction to spectral regions free of Galactic absorption lines. The power law has the form $F_\lambda = 3.31 \times 10^{-15}(\lambda/1000\ \text{Å})^{-2.40}$ erg cm^{-2} s^{-1} Å^{-1}. We used a mean Galactic extinction curve with $R_V = 3.1$ and $E(B-V) = 0.014$ (Cardelli et al. 1989; Schlegel et al. 1998). Figure 1 shows a portion of the STIS spectrum where it overlaps our *FUSE* spectrum, and the fitted continuum. This extrapolated continuum is used in our opacity calculations below.

Examination of Figure 1 immediately shows several qualitative characteristics of absorption by ionized He in the IGM. At redshifts above $z = 2.72$ ($\lambda \gtrsim 1130$ Å), the IGM is relatively opaque, with occasional narrow windows that are nearly transparent (Reimers et al. 1997; Smette et al. 2001). At $z = 2.72$, the IGM becomes more transmissive, and the opacity systematically drops at lower redshifts and shorter wavelengths. In this translucent region, one can also see that discrete absorption features account for most, if not all, of the opacity—we have resolved the ionized He absorption into a He II Lyα forest, analogous to the H I Lyα forest.

The quantitative character of this evolution in opacity with redshift is consistent with our expectations. The mean opacity over the redshift interval 2.3–2.7 is $\tau_{\rm HeII} = 0.91 \pm 0.01$, similar to the sightline towards HS1700+64 (Davidsen et al. 1996). (While the *mean* opacity is tightly constrained, we note that there is a large dispersion of 0.9 about this value.) Figure 2 shows the mean opacity as a function of redshift. The chosen bins avoid airglow lines and detector gaps, and they isolate the windows of low opacity at higher redshift. The figure also compares the measured opacities to a model of its evolution

as expected for discrete clouds photoionized by the general quasar population, valid for epochs after He II re-ionization is complete (Fardal et al. 1998). In the model, ionization fluctuations on scales of ~4000 km s^{-1} (~15 Å, the size of our largest bins) lead to the predicted range of opacities shown in the figure. One sees that for $z < 2.72$, where He II reionization is potentially complete, the absolute level of the observed opacity, its trend to lower values at lower redshift, and the fluctuations about the mean are all consistent with this model.

The extrapolated STIS continuum provides an excellent fit to the peak fluxes in the *FUSE* spectrum. Positive residuals from points above the extrapolated continuum have a Gaussian distribution consistent with the 1σ error bars on our data points, indicating that there are absorption-free windows where the IGM is completely transparent in He II Lyα. These peaks set limits on absorption by smoothly distributed gas in the IGM. For the specific model of a constant co-moving density of $n_{\rm HeII} \propto (1+z)^3$ and a $\Lambda = 0$ cosmology with $\Omega = 1$, the opacity in smoothly distributed He II Lyα varies with redshift as $\tau_{\rm HeII} = \tau(z = 2.885)[(1+z)/(1+2.885)]^{4.5}$ for $z < 2.885$ (Gunn & Peterson 1965). By requiring that the distribution of positive residuals be consistent with a Gaussian of mean 0 and dispersion 1, we set a 1-σ upper limit on $\tau(z = 2.885)$ by permitting $\tau(z = 2.885)$, the power law index, and its normalization to vary freely until χ^2 increases by 1. This yields an upper limit of $\tau(z = 2.885) < 0.11$.

Since the *FUSE* data resolve the He II Lyα forest, there is much we can learn from a more detailed examination of the individual absorption features and a comparison to their counterparts in the H I Lyα forest. To measure the individual He II column densities, we fit the *FUSE* spectrum using the spectral fitting task SPECFIT (Kriss 1994). Our model incorporates the extrapolated continuum, individual He II absorption lines with Voigt profiles (assuming $b_{\rm HeII} = b_{\rm HI}$), and foreground interstellar absorption in our own

Galaxy. (For the low extinction along this sightline, the interstellar absorption model contributes significant features only for Lyβ λ1025, Si II λ1026, C II λ1036, O I λ1039, Ar I $\lambda\lambda$1048, 1066, and no significant H_2 absorption (*Footnote1*).) For each He II line, we permit the column density to vary freely, but we fix the redshift and the line width ($b_{\rm HeII} = b_{\rm HI}$) to have the same values as those in the H I line list from a Keck observation of HE2347–4342 with a resolution of 8 km s^{-1} (Songaila 1998). The H I lines identified in the Keck spectrum (184 in total) all have He II counterparts. Although these lines account for most of the observed opacity in He II Lyα, they account for only $\sim$50% of the observed features. To model the remaining features, we inserted additional lines whose redshifts were permitted to vary freely and whose widths were fixed at b = 27 km s^{-1}, the mean of the distribution from the H I line list. Over the 1000–1130 Å wavelength range, 179 additional He II Lyα absorption features were added to our fit. At the 3-σ confidence limit, we are sensitive to He II lines with a limiting column density of log N(HeII) > $10^{12.8}$ cm^{-2}. For comparison, there are 72 H I Lyα features with $N_{\rm HI} < 10^{13}$ cm^{-}2 in the same corresponding redshift range in the Keck spectrum. To illustrate the excellent correspondence between the H I features visible in a Keck spectrum of HE2347–4342 and the He II absorption visible in the *FUSE* spectrum, Figure 3 compares a small portion of the fitted *FUSE* spectrum to the corresponding redshift region in the Keck spectrum.

The added features are consistent with a short extrapolation of the number of H I lines per unit column density of the form $f(N_{HI}) \propto N_{HI}^{-1.5}$ (Press & Rybicki 1993; Hu et al. 1995; Fardal et al. 1998) down to column densities of $\sim 10^{11}$ cm^{-2}. This is potentially a substantial amount of material, but, given the power law form of the column density distribution, it probably does not dominate the total mass in the Lyα forest (Bi & Davidsen 1997; Shull et al. 2001). Given that the physical sizes of the absorbers and the ionization corrections are highly uncertain, we refrain from estimating the amount of mass that this population of absorbers represents. However, in the context of

hydrodynamical models of the IGM (Croft et al. 1997; Bi & Davidsen 1997), we note that ∼10% of the baryons at redshifts of 2–3 should reside in the low-column density extension of the Lyα forest.

With measured column densities in discrete features in both He II and H I, we can infer the shape of the ionizing spectrum illuminating the absorbing gas. Figure 4 shows the ratio of He II to H I column densities, η = N(HeII)/N(HI). Points with both He II and H I measurements have a mean value $< \log \eta >= 1.47 \pm 0.05$. Since our data include both measured values and lower limits (for He II Lyα features with no H I Lyα counterparts), we use the Kaplan-Meier estimator for censored data (Feigelson & Nelson 1985) to derive a mean value for the full data set of $< \log \eta >= 1.89 \pm 0.04$. Models of an IGM photoionized by the integrated light from quasars propagated through the IGM (Fardal et al. 1998; Madau et al. 1999) predict values of $\eta = 30 - 70$ for input quasar spectra with spectral indices $\alpha_q = 1.5 - 1.8$ (for $f_\nu \propto \nu^{-\alpha_q}$). Intrinsic spectral indices for quasars (as measured down to a rest wavelength of ∼350 Å) lie in this range (Zheng et al. 1997; Telfer et al. 2001). Thus, most of the observed absorption features appear to be consistent with photoionization by quasar radiation. There is a significant population of absorbers, however, with values of $\eta > 100$, indicating that localized regions of the IGM are photoionized by softer spectra. This might either be heavily filtered quasar radiation (in regions where the re-ionization of He II is not yet complete), or stellar radiation from sites of ongoing star formation (e.g., see the models in (Fardal et al. 1998)).

By examining Figure 4, one can see significant fluctuations in η on scales of $\Delta z \sim 0.01$. This implies that the ionizing radiation field is not uniform. Local radiation sources (which may be either quasars or star-forming galaxies) and their individual spectral shapes probably affect η and the local opacity of the IGM. This characteristic is most evident at high redshift in the low-opacity "windows" first seen in *HST* spectra of HE2347–4342

(Reimers et al. 1997; Smette et al. 2001), but it persists to lower redshift where the IGM is less opaque. We will explore these ideas further in a future publication (Shull et al. 2001).

In summary, our *FUSE* observation of the quasar HE2347–4342 resolves the He II absorption in the IGM as a "He II Lyα forest", analogous to the H I Lyα forest seen in optical spectra of high-redshift quasars. As for H I, any smoothly distributed component of the He II absorption is undetectable, to an upper limit of $\tau \lesssim 0.1$. The observed structure of the IGM is consistent with the predictions of hydrodynamical models of the evolution of structure in the universe in which a significant fraction of the He II Lyα opacity arises in low-density regions without much H I Lyα absorption. The ionization state fluctuates significantly from absorber to absorber. Most have N(He II)/N(H I) ratios of 1–80, consistent with photoionization by the integrated light from quasars propagating through the IGM, but there are large fluctuations to values exceeding 100. These regions must be photoionized by softer spectra which may be either heavily filtered QSO radiation or the light of newly formed stars.

REFERENCES

Bi, H., *Ap.J.* **405**, 479 (1993).

Bi, H., & Davidsen, A. F., *Ap.J.* **479**, 523 (1997).

Bi, H., Ge, J., & Fang, L.-Z., *Ap.J.* **452**, 90 (1995).

Cardelli, J., Clayton, G., & Mathis, J. *Ap.J.* **345**, 245 (1989).

Cen, R., Miralda-Escudé, J., Ostriker, J. P., & Rauch, M. *Ap.J.* **437**, L9 (1994).

Cen, R., & Ostriker, J. P., *Ap.J.* **514**, 1 (1999).

Croft, R.A.C., Weinberg, D.H., Katz, N., & Hernquist, L., *Ap.J.* **488**, 532 (1997).

Davé, R., Hernquist, L., Katz, N., & Weinberg, D. H. *Ap.J.* **511**, 521 (1999).

Davidsen, A.F., Kriss, G.A., & Zheng, W., *Nature* **380**, 47 (1996).

Fardal, M.A., Giroux, M.L., & Shull, J.M., *A.J.* **115**, 2206 (1998).

Feigelson, E.D., & Nelson, P.I., *Ap.J.* **293**, 192 (1985).

Gunn, J., & Peterson, B., *Ap.J.* **142**, 1633 (1965).

Heap, S. R., et al., *Ap.J.* **534**, 69 (2000).

Hernquist, L., Katz, N, Weinberg, D. H., & Miralda-Escudé, J. *Ap.J.* **457**, L51 (1996).

Hu, E. M., Kim, T.-S., Cowie, L. L., Songaila, A., & Rauch, M., *A.J.* **110**, 1526 (1995).

Hui, L., Gnedin, N. Y., & Zhang, Y., *Ap.J.* **486**, 599 (1997).

Jakobsen, P., et al., *Ap.J.* **417**, 528 (1993).

Jakobsen, P., et al., *Nature* **370**, 35 (1994).

Kriss, G. A., in Astronomical Data Analysis Software and Systems III, A.S.P. Conf. Series, V. 61, ed. D. R. Crabtree, R. J. Hanisch & J. Barnes (San Francisco: ASP), 437 (1994).

Lynds, R. *Ap.J.* **164**, L73 (1971).

Madau, P., Haardt, F., & Rees, M.J. *Ap.J.* **514**, 648 (1999).

Miralda-Escudé, J., Cen, R., Ostriker, J. P. & Rauch, M., *Ap.J* **471**, 582 (1996).

Moos, H. W., et al., *Ap.J.* **538**, L1 (2000).

Press, W. H., & Rybicki, G. B.,*Ap.J.* **418**, 585 (1993).

Reimers, D., et al., *A&A* **327**, 890 (1997).

Sahnow, D., et al., *Ap.J.* **538**, L7 (2000).

Schlegel, D. J., Finkbeiner, D. P., & Davis, M., *Ap.J.* **500**, 525 (1998).

Shull, J. M., et al., *Ap. J.*, in preparation (2001).

Smette, A., Heap, S.R., Williger, G.M., Tripp, Jenkins, E.B., Songaila, A., *Ap.J.*, in press (astro-ph/0012193) (2001).

Songaila, A., Hu, E.M., Cowie, L.L., *Nature* **375**, 124 (1995).

Songaila, A., *A.J.* **115**, 2184 (1998).

Telfer, R.C., Zheng, W., Kriss, G.A., & Davidsen, A. F., 2001, in prep.

Zhang, Y., Anninos, P., & Norman, M.L., *Ap.J.* **453**, L57 (1995).

Zhang, Y., Anninos, P., Norman, M.L., & Meiksin, A., *Ap.J.* **485**, 496 (1997).

Zheng, W., Kriss, G.A., Telfer, R. C., Grimes, J. P., & Davidsen, A. F. *Ap.J.* **475**, 469 (1997).

Zheng, W., Davidsen, A.F. & Kriss, G.A., *A.J.* **115**, 391 (1998).

Footnote1. Along similar high latitude sight lines observed with *FUSE*, the column density in H_2 is of order a few $\times 10^{15}$ cm^{-2}. The average opacity produced by such a column density amounts to $< 4\%$ from 1000–1110 Å.

Acknowledgments. This work is based on data obtained for the Guaranteed Time Team by the NASA-CNES-CSA *FUSE* mission operated by the Johns Hopkins University. Financial support to U. S. participants has been provided by NASA contract NAS5-32985, and by the NASA LTSA grant NAG5-7262 to the University of Colorado. A portion of this work is based on observations with the NASA/ESA *Hubble Space Telescope*, obtained at the Space Telescope Science Institute, which is operated by the Association of Universities for Research in Astronomy, Inc., under NASA contract NAS5-26555. These observations are associated with proposal ID 8875. We thank B. Roberts for his efforts in planning and scheduling the successful *FUSE* observations.

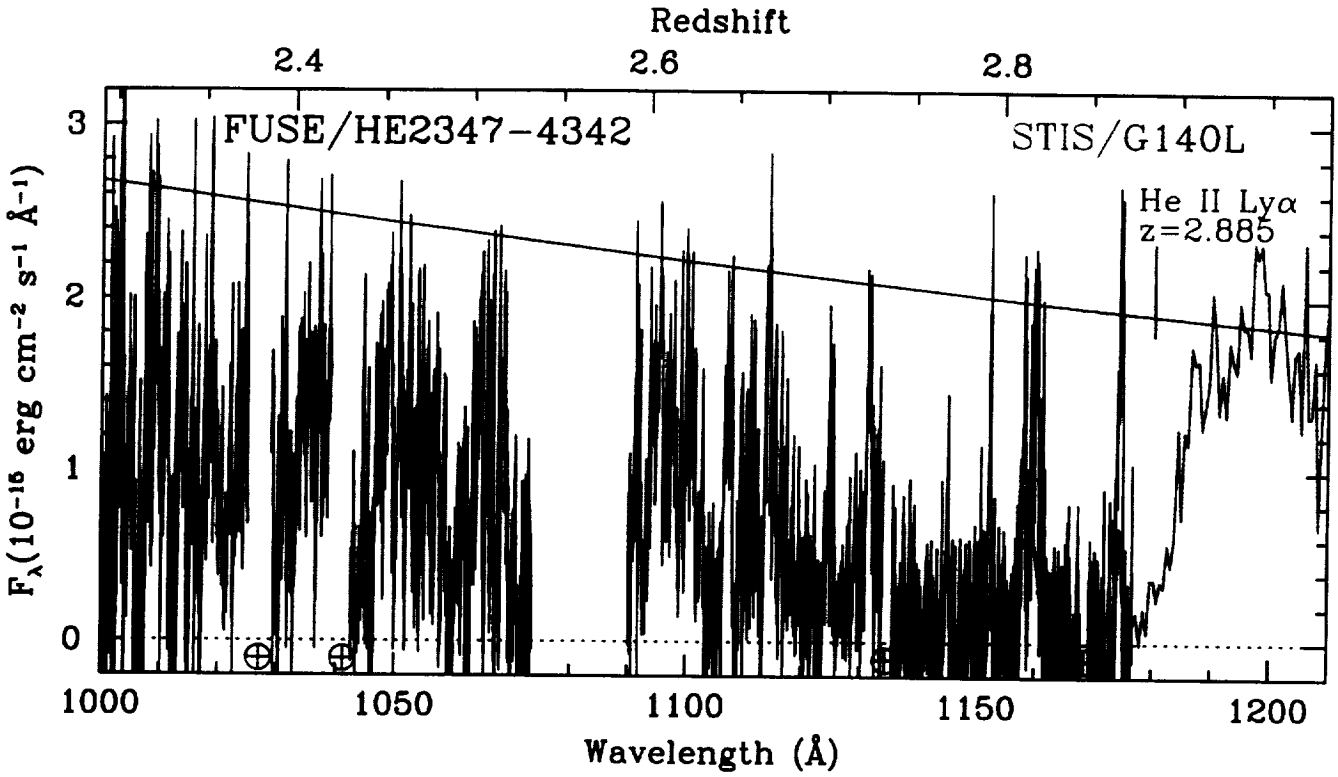

Fig. 1.— *FUSE* spectrum of HE2347–4342 (binned to 0.05 Å pixels) is shown in black. A portion of the contemporaneous STIS spectrum is shown in green. The red line is the extrapolation of the power law plus extinction of E(B-V)=0.014 fitted to the STIS spectrum. The position of He II Lyα at the redshift of HE2347–4342 is marked. Gaps in the *FUSE* spectrum due to excised terrestrial airglow lines are marked with green $\oplus$. The broad gap from 1072–1089 Å is due to gaps between the *FUSE* detector segments for channels LiF1 and LiF2.

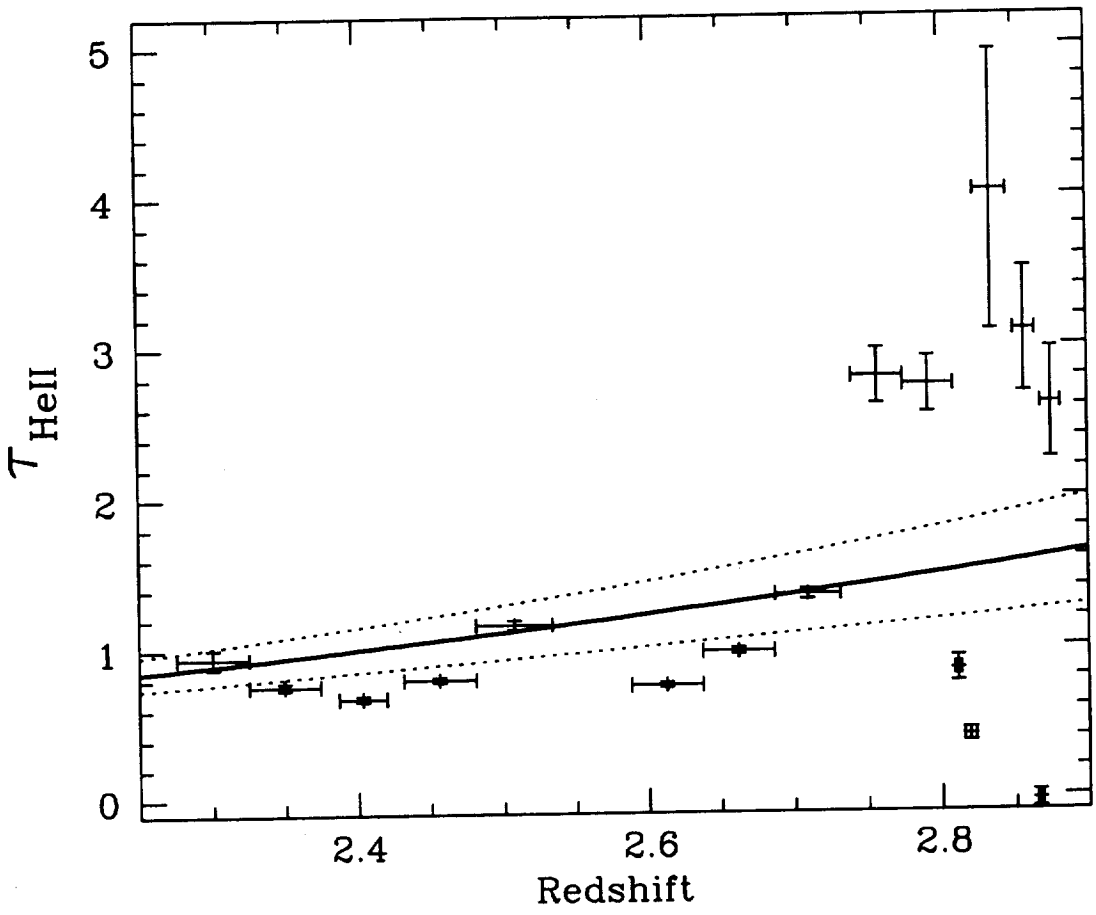

Fig. 2.— The He II opacity τ_{HeII} in coarse 5–15 Å bins is shown as a function of redshift. The solid curve is the theoretical prediction for the opacity assuming line blanketing only (Fardal et al. 1998). The dotted curves indicate the 1 σ extent of variations in the opacity anticipated due to ionization fluctuations. At redshifts below $z = 2.72$, where the reionization of He II in the IGM appears to be complete, the model matches well the observed opacity, its trend to lower values at lower redshift, and the fluctuations about the mean.

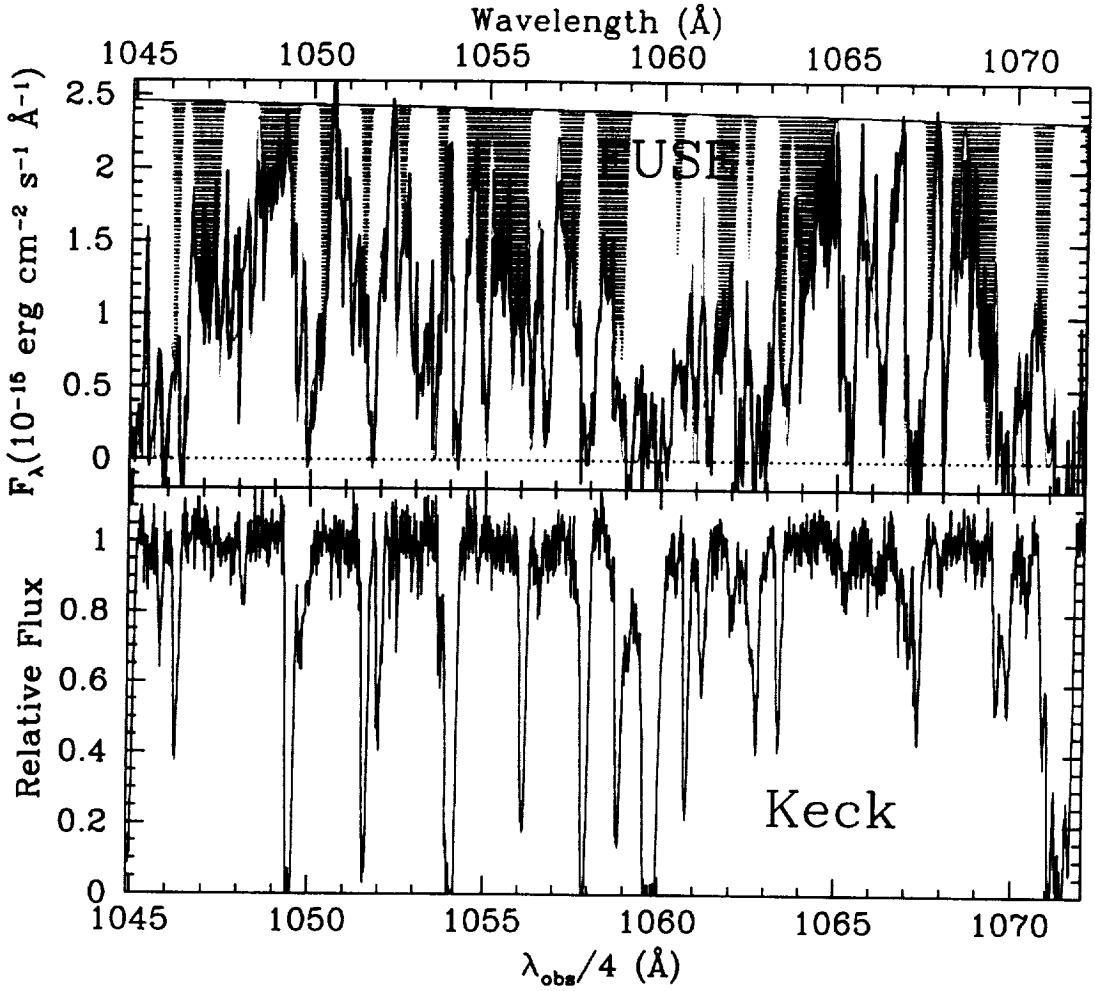

Fig. 3.— Top panel: The black line is a portion of the *FUSE* spectrum of HE2347–4342. The smooth red curve across the top is the extrapolated continuum. The magenta line overlaying the spectral data in black is the model described in the text. The area shaded in yellow shows the fraction of the He II opacity due to absorption features that correspond to H I absorption lines identified in the Keck spectrum (Songaila 1998). The area shaded in green shows the fraction of the opacity due to additional He II absorption features that have no H I counterparts in the Keck spectrum. Bottom panel: the normalized Keck spectrum (Songaila 1998). Note the direct correspondence between H I lines in the Keck spectrum and He II absorption features in the *FUSE* spectrum.

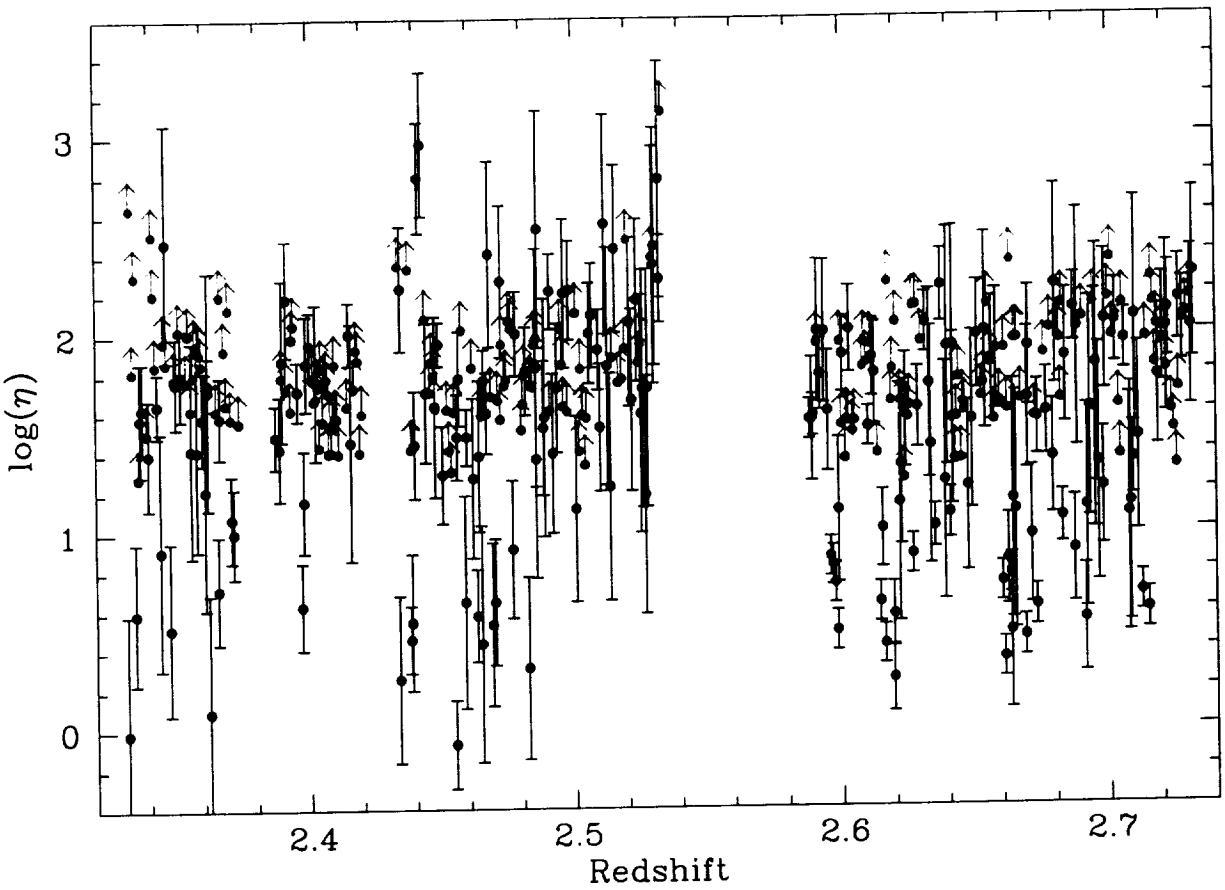

Fig. 4.— The logarithm of the He II to H I column density ratio η=N(HeII)/N(HI) vs. redshift for measured absorption features in the *FUSE* spectrum. The black points with error bars have measured column densities for both HeII (from *FUSE*) and H I (from Keck). The red points are lower limits computed using the He II column density measured from the *FUSE* spectrum and an upper limit of $10^{12.3}$ cm^{-2} for H I absorption lines in the Keck spectrum. There is no significant trend with redshift. Taking the distribution of lower limits into account (Feigelson & Nelson 1985), $< \log \eta >= 1.89 \pm 0.04$, consistent with photoionization of the IGM by integrated quasar light (Fardal et al. 1998; Madau et al. 1999). However, one can see significant fluctuations in η that indicate that the ionizing radiation field is not uniform. Values of $\eta > 100$ indicate regions photoionized by either heavily filtered quasar radiation or bursts of star formation.